iScience

CellPress

Article

Room Temperature Processing of Inorganic Perovskite Films to Enable Flexible Solar Cells

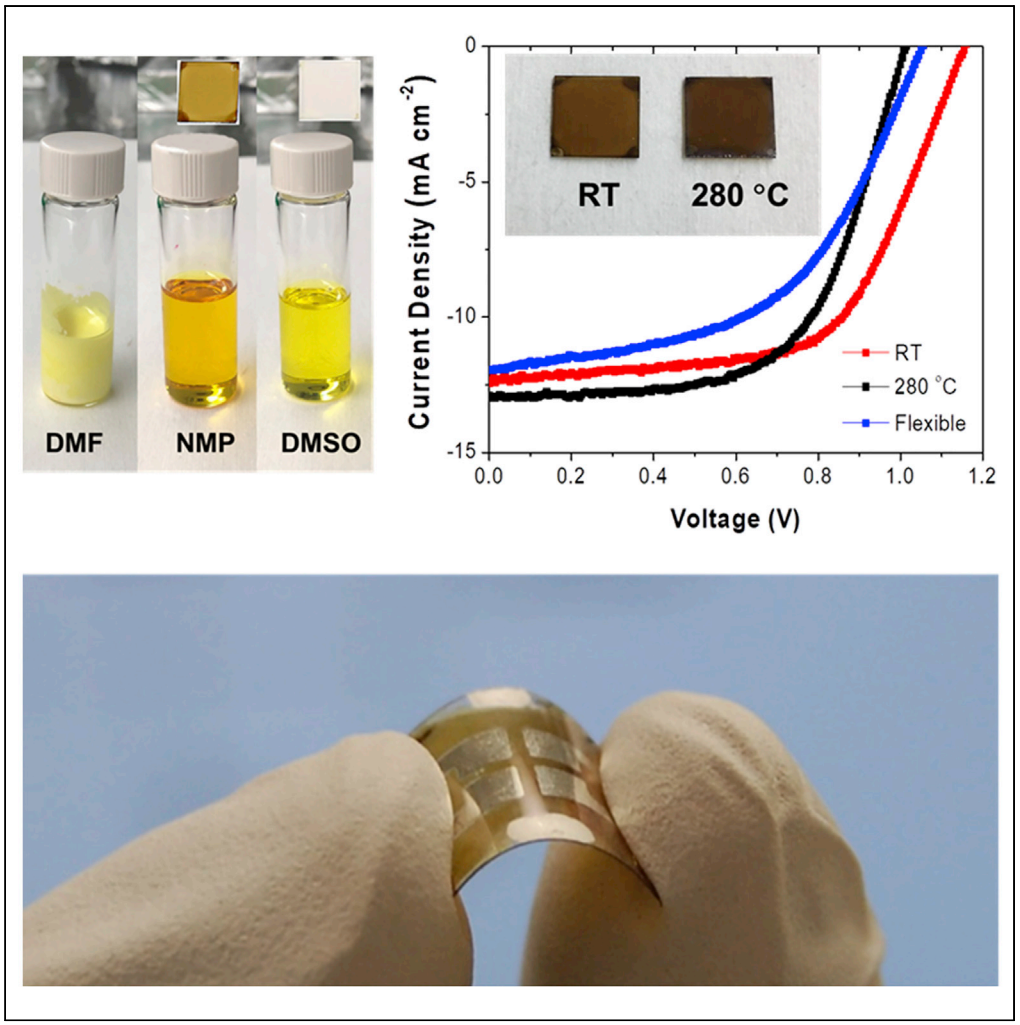

Dianyi Liu, Chenchen Yang, Matthew Bates, Richard R. Lunt

rlunt@msu.edu

HIGHLIGHTS

Developed room temperature processing of inorganic PSCs based on $CsPbI_2Br$

Flexible inorganic PSCs based on an inorganic metal halide perovskite are demonstrated

Films show improved humidity stability compared with films annealed at high temperature

Power conversion efficiencies up to 8.67% and 6.50% for rigid and flexible devices

Liu et al., iScience 6, 272–279
August 31, 2018
https://doi.org/10.1016/j.isci.2018.08.005

iScience

CellPress

Article

Room Temperature Processing of Inorganic Perovskite Films to Enable Flexible Solar Cells

Dianyi Liu,[1] Chenchen Yang,[1] Matthew Bates,[1] and Richard R. Lunt[1,2,3,*]

SUMMARY

Inorganic lead halide perovskite materials have attracted great attention recently due to their potential for greater thermal stability compared with hybrid organic perovskites. However, the high processing temperature to convert from the non-perovskite phase to the cubic perovskite phase in many of these systems has limited their application in flexible optoelectronic devices. Here, we report a room temperature processed inorganic perovskite solar cell (PSC) based on $CsPbI_2Br$ as the light harvesting layer. By combining this composition with key precursor solvents, we show that inorganic perovskite films can be prepared by the vacuum-assist method under room temperature conditions in air. Unencapsulated devices achieved power conversion efficiency up to 8.67% when measured under 1-sun irradiation. Exploiting this room temperature process, flexible inorganic PSCs based on an inorganic metal halide perovskite material are demonstrated.

INTRODUCTION

Halide perovskite materials have emerged as excellent candidates for photovoltaic applications in recent years (Burschka et al., 2013; Kojima et al., 2009; Liu et al., 2013; Zhou et al., 2014). High device efficiency and low materials costs have given perovskite solar cells (PSCs) strong potential as a competitor for silicon solar cells (Liu and Kelly, 2014; Mei et al., 2014; Yang et al., 2017). To date, the highest reported power conversion efficiency (*PCE*) of hybrid organic-inorganic PSCs is up to 22.7% (Yang et al., 2017), which is higher than the efficiencies of polycrystalline silicon solar cells, cadmium telluride solar cells, and copper-indium-gallium selenide solar cells. However, the stability issue of organic-inorganic halide perovskite materials is still a key challenge for the commercial application of PSCs due to the high volatility of organic components in hybrid perovskite compounds (Eperon et al., 2014; Gratzel, 2014; Leijtens et al., 2015).

In contrast, inorganic perovskite materials could have better intrinsic thermal stability (Sharma et al., 1992). Previous research suggests that the pure $CsPbI_3$ perovskite can maintain a stable cubic phase over 400°C (Sharma et al., 1992; Sutton et al., 2016). Thus, significant effort has been focused on developing PSCs with the inorganic cesium lead halide light absorbers (Beal et al., 2016; Chen et al., 2017; Frolova et al., 2017; Li et al., 2017; Liang et al., 2016; Ma et al., 2017; Nam et al., 2017a, 2017b; Niezgoda et al., 2017; Sutton et al., 2016; Swarnkar et al., 2016; Zeng et al., 2018; Zhang et al., 2018a). Sutton et al. systematically investigated the stability behavior of the cesium lead halide compounds and reported inorganic PSCs with a *PCE* of 9.84% (Sutton et al., 2016). Chen et al. used the vacuum-deposition method to prepare inorganic cesium halide PSCs and achieved a device efficiency over 11% (Chen et al., 2017). Zeng et al. reported a polymer-passivated cesium lead halide PSC based on inorganic perovskite nanocrystals with a *PCE* of over 12% and an open-circuit voltage (V_{OC}) of over 1.3 V (Zeng et al., 2018). Wang et al. very recently reported a certified efficiency of 14.67%, which is also the highest efficiency of inorganic PSCs to date (Wang et al., 2018). Despite the rapid research progress in improving efficiencies with inorganic PSCs, the processing of inorganic perovskite film is still challenging. Because the conversion temperature of $CsPbI_3$ from the non-perovskite phase to the cubic perovskite phase occurs at over 300°C (Sharma et al., 1992; Sutton et al., 2016), the fabrication process of $CsPbI_{3-x}Br_x$-based inorganic perovskite films generally requires a thermal annealing treatment at temperatures up to 350°C (Chen et al., 2017; Duan et al., 2018; Frolova et al., 2017; Liang et al., 2016; Nam et al., 2017a, 2017b; Niezgoda et al., 2017; Sutton et al., 2016; Zeng et al., 2018; Zhang et al., 2018a). The high temperature thermal annealing treatment not only increases the cost of inorganic PSCs but also can prevent the application of inorganic perovskite materials on polymer-based flexible substrates.

[1]Department of Chemical Engineering and Materials Science, Michigan State University, East Lansing, MI 48824, USA

[2]Department of Physics and Astronomy, Michigan State University, East Lansing, MI 48824, USA

[3]Lead Contact

*Correspondence: rlunt@msu.edu

https://doi.org/10.1016/j.isci.2018.08.005

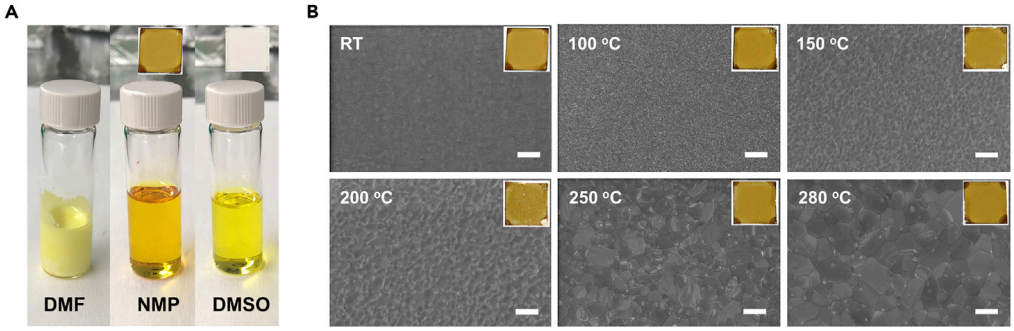

Figure 1. Characterization of $CsPbI_2Br$ Precursor Solutions and Films

(A) Photograph of $CsPbI_2Br$ precursor solutions prepared by various solvents. The inset shows the films prepared by the corresponding precursor solutions with the room temperature process.

(B) Scanning electron micrograph of $CsPbI_2Br$ films with various annealing temperatures. The inset shows the photograph of the films. Scale bar, 1 μm.

To reduce the operation temperature of cesium lead halide perovskite films, several approaches have been examined in the past 2 years (Akkerman et al., 2016; Beal et al., 2016; Eperon et al., 2015; Hu et al., 2017; Luo et al., 2016; Wang et al., 2017c, 2017d; Zhang et al., 2017). For example, it was shown that doping a small amount of bromide (Br) can dramatically decrease the formation temperature of $CsPbI_3$ films (Yin et al., 2014). Following this work, Beal et al. reported the low-temperature processing of $CsPbBrI_2$ films as the light absorber (Beal et al., 2016). The device was fabricated at 135°C and achieved a *PCE* of up to 6.5%. Other efforts have introduced various additives to decrease the fabrication temperature, which include hydroiodic acid, bismuth iodide, sulfobetaine zwitterions, and ethylammonium iodide (Eperon et al., 2015; Hu et al., 2017; Luo et al., 2016; Wang et al., 2017c, 2017d; Zhang et al., 2017). With these additives, the cubic phase $CsPbI_{3-x}Br_x$ film could be formed at 90°C–150°C. However, the thermal annealing treatment still remained an essential step for preparation of the cesium lead halide perovskite films.

Room temperature processing is not only important to simplify the fabrication procedure but also enables fabrication on flexible substrates (Liu and Kelly, 2014). To date, only a couple of studies have reported inorganic lead halide films fabricated under room temperature that then required high-temperature annealing of TiO_2 (450°C–500°C) and pre-synthesized perovskite quantum dots (Akkerman et al., 2016; Swarnkar et al., 2016). In addition, despite many reports of flexible solar cells based on the organic-inorganic hybrid perovskite materials, flexible inorganic PSCs have not yet been reported (Bi et al., 2017; Docampo et al., 2013; He et al., 2017; Kaltenbrunner et al., 2015; Li et al., 2018; Ling et al., 2017; Liu and Kelly, 2014; Remeika et al., 2018; Roldan-Carmona et al., 2014; Wang et al., 2017a; Zhang et al., 2016, 2018b). Here, we develop a room temperature processed inorganic PSC with $CsPbI_2Br$ as the light harvesting layer. By choosing a suitable precursor solvent, combined with the vacuum-assist method, we show that inorganic perovskite films can be prepared at room temperature in air with a *PCE* up to 8.67% when measured at 1-sun irradiation. We subsequently show that this low-temperature processing enables fabrication of highly flexible inorganic halide perovskite photovoltaics.

RESULTS AND DISCUSSION

Due to the limited solubility of lead halide compounds, the precursor solvents generally chosen are N,N-dimethylformamide (DMF), DMSO, and DMF/DMSO mixtures (Burschka et al., 2013; Chen et al., 2016; Jeon et al., 2014; Liu et al., 2018a, 2018b; Zhou et al., 2014). The solubility of mixed halide cesium lead precursors are particularly limited in DMF (Figure 1A) (Sutton et al., 2016), leading some researchers to utilize pure DMSO (Beal et al., 2016; Hu et al., 2017; Li et al., 2017; Wang et al., 2017c; Zhang et al., 2018a). However, DMSO is a Lewis base with strong coordination capability, which can result in colorless coordination complexes with lead halide compounds (Ahn et al., 2015; Jeon et al., 2014; Jo et al., 2016; Lee and Baik, 2018; Wu et al., 2014) and can lead to difficulties in converting the lead halide perovskite precursors to the perovskite phase under room temperature (Figure 1A). Another polar aprotic solvent used to fabricate organic-inorganic hybrid PSCs is 1-methyl-2-pyrrolidone (NMP) (Hao et al., 2015; Jo et al., 2016; Nie et al., 2015; Tsai et al., 2017; Zhou et al., 2015). Compared with DMF and DMSO, NMP has good solubility for cesium lead halide precursors and weak coordination affinity for lead compounds. NMP has other advantages as well,

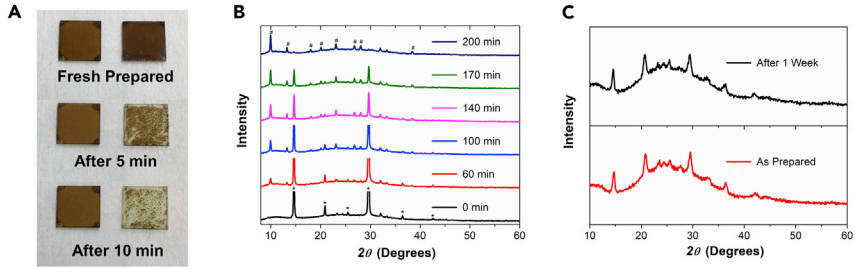

Figure 2. Stability Characterization of $CsPbI_2Br$ Films

(A) Photograph of $CsPbI_2Br$ films stored under ambient air with RH = 30% ± 4%. The left row is the room temperature film, and the right row is the film with 280°C annealing treatment.

(B) XRD patterns of the film with 280°C annealing treatment measured continuously in ambient air with RH = 22% ± 4%. Perovskite peaks are denoted with a "#" and decomposition products are denoted with a "*".

(C) XRD patterns of the room temperature film before and after storage in ambient air with RH ≤ 22% ± 4% for a week.

including better crystallization of perovskite films and miscibility with other solvents, and has been reported as the solvent to fabricate hybrid organic-inorganic PSCs under room temperature (Tsai et al., 2017; Zhou et al., 2015). Hence, we focus on NMP as the solvent for the preparation of inorganic lead halide perovskite films with room temperature processing.

It can be seen from Figure 1A that the CsPbI2Br perovskite films can be successfully prepared by the vacuum-assist deposition process under room temperature (Li et al., 2016; Liu et al., 2018a, 2018b). After the NMP solvent was extracted from the film under vacuum, the light brown $CsPbI_2Br$ perovskite film was formed. Scanning electron micrographs (Figure 1B) show that the $CsPbI_2Br$ film is smooth and homogeneous. Due to the rapid solvent extraction the $CsPbI_2Br$ film was formed quickly with a low level of crystallization, and led to a grain size of ~50 nm. To investigate the thermal stability of the room temperature processed $CsPbI_2Br$ film, we annealed the films under various temperatures in an inert atmosphere. The photograph of these films clearly shows that the films maintain a brown color from room temperature to 280°C. The color of the 100°C film and the 150°C film are different from the previous report by Sutton (Sutton et al., 2016), but agree with the report by Beal (Beal et al., 2016). We infer that the film preparation method can dramatically influence the phase conversion temperature and the thermal stability of $CsPbI_2Br$ films. Accordingly, the scanning electron micrographs clearly indicate that the grain size of $CsPbI_2Br$ films gradually increased from ~50 nm at room temperature to ~1 μm at 280°C (Figure S1).

The as-prepared $CsPbI_2Br$ films with various annealing temperatures are also investigated by absorption spectroscopy and powder X-ray diffraction (XRD) (Figure S2). The absorption spectra show that all the films have strong absorption from 300 to 650 nm wavelength range (Figure S2A). After being annealed, the absorption of films presents a peak at 640 nm.

XRD patterns (Figure S2C) show that at room temperature the film has cubic perovskite peaks at 2θ = 14.7, 20.9, 29.6, and 42.6°, which are indexed to the (100), (110), (200), and (220) planes of $CsPbI_2Br$, respectively. After being annealed, these diffraction peaks become stronger and sharper, which confirms the improved crystallization of the perovskite films. It is important to note that when the film is annealed to 150°C–250°C, new peaks at 2θ = 12.7 and 38.8° are observed. Since the new peaks are in agreement with the diffraction peaks of PbI_2 (Liu et al., 2014), we infer that a small amount of $CsPbI_2Br$ subsequently decomposes. However, the film can maintain a metastable cubic phase up to 150°C (Figures S3 and S4). We suspect that this is due to structural tolerance factors that are close to the borderline of stable perovskite phases. This is reflected in the slight variation in the lattice constants found for the phases formed at room temperature (a = 6.11 Å) and 280°C (a = 6.02 Å). Because the lattice constant of the room temperature phase is larger, this implies that the ionic radius of Pb(II) or Br is slightly larger, leading to a reduced tolerance factor compared with the cubic phase obtained from high-temperature processing.

The humidity stability of $CsPbI_2Br$ films prepared at room temperature and 280°C was also investigated. Figure 2A is the photograph of $CsPbI_2Br$ films before and after a short period (10 min) of storage under relative humidity (RH) of 30% ± 4% in open air, respectively. It is clear that the room temperature processed film can maintain the brown color. In contrast, the 280°C film changes color in only 5–10 min, which suggests

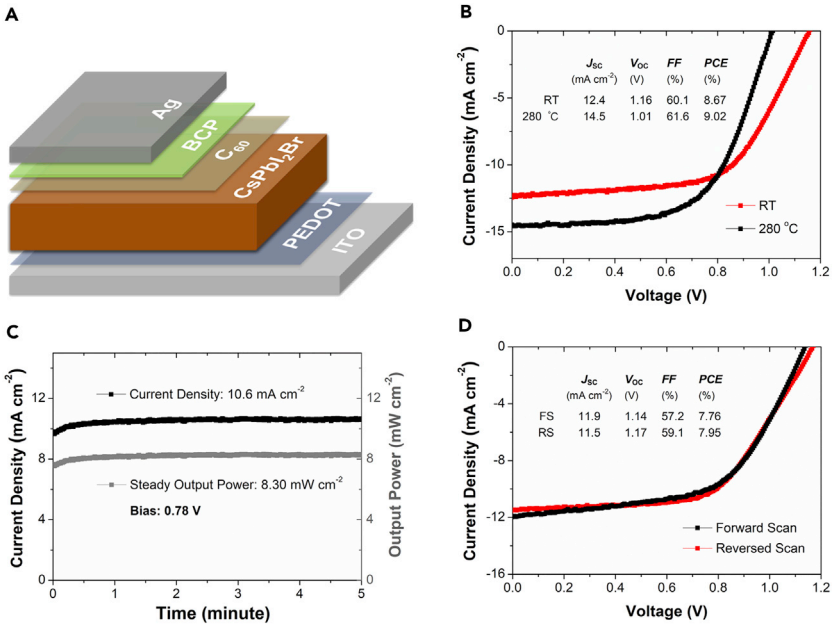

Figure 3. Device Architecture and Performance

(A) PSC device architecture.

(B) Current-voltage (*J-V*) curves of perovskite devices with room temperature $CsPbI_2Br$ film and 280°C annealing treatment film measured under 1-sun illumination, respectively.

(C) The steady current density and power output under 1-sun illumination at a bias of 0.78 V.

(D) The *J-V* curves of room temperature processed $CsPbI_2Br$ device (different devices within B and C) measured with reverse and forward bias.

that the film undergoes a phase change or decomposition. The scanning electron micrograph for the room temperature processed $CsPbI_2Br$ film after storage has no obvious change (Figure S5). In comparison, the 280°C film shows a clear change with the formation of pinholes on the film surface after storage.

To further investigate the phase change of the 280°C film under humidity, we continuously measured the XRD spectra of the film under room temperature and RH = 22% $\pm$ 4% in air (Figure 2B). The initially prepared 280°C film shows the characteristic cubic perovskite peaks. During exposure to humidity, the cubic peaks begin to fade, whereas new diffraction peaks at 2θ = 10.0, 13.3, 26.8, 28.1, and 38.4° emerge. After 200 min the peaks of cubic phase completely disappear. In contrast, no change is observed in the XRD spectra for the room temperature processed $CsPbI_2Br$ film for over 1 week (Figure 2C). This indicates that the room temperature processed film has improved humidity stability and will therefore likely lead to improved operational lifetime as well.

Films with larger grain size are generally more compact than those with small grain size, and the more compact film should have better stability because of the better resistance to degradation from moisture and oxygen (Liu et al., 2018a). However, recent studies suggest that cesium lead halide perovskite films with small grain size have significantly improved stability than films with larger grain size (Wang et al., 2017c; Zhang et al., 2017). The reduction in the number of pinholes and defect passivation on the surface are believed to be the main contributions to the improved stability. Our observation is consistent with these studies. Previous studies also have found that grain boundaries play an important role in the perovskite film degradation process (Wang et al., 2017b; Yun et al., 2018). Chemical residues at the grain boundaries are suggested to be one possible reason for accelerated degradation of perovskite films. Overall, the room temperature processed technique provides an effective approach to improve the humidity stability of $CsPbI_2Br$ films.

Subsequently, the room temperature processed $CsPbI_2Br$ solar cells were prepared with the architecture shown in Figure 3A. An ultrathin poly(3,4-ethylenedioxythiophene)-poly(styrenesulfonate) (PEDOT) layer

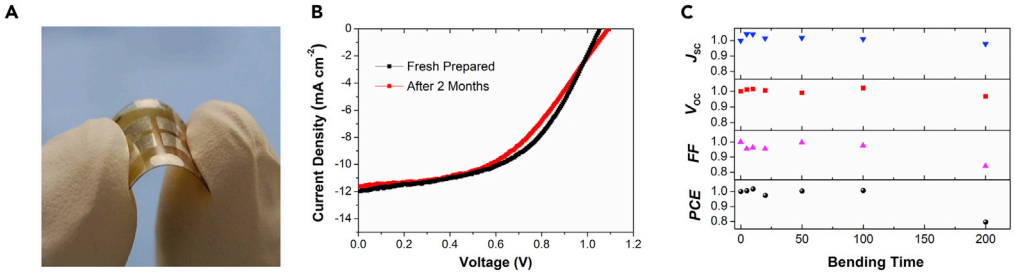

Figure 4. Photograph and Performance of Flexible PSCs

(A) Photograph of a flexible $CsPbI_2Br$ device.

(B) *J-V* curves of the champion flexible $CsPbI_2Br$ device measured before and after 2 months storage in a glove box without any encapsulation.

(C) Normalized parameters of flexible $CsPbI_2Br$ devices under various bending cycleswith a bending radius of 4.05 mm.

was first deposited on pre-cleaned indium tin oxide (ITO) substrates. The $CsPbI_2Br$ layer was then prepared on top of the PEDOT layer by the vacuum-assist method in ambient atmosphere (Liu et al., 2018a, 2018b). A 20-nm C_{60} and a 7.5-nm 2,9-dimethyl-4,7-diphenyl-1,10-phenanthroline layer were then thermally evaporated onto the $CsPbI_2Br$ layer followed by the silver electrode.

The current-voltage (*J-V*) characteristics of the devices are shown in Figure 3B. Under standard AM1.5G illumination, the room temperature processed device shows a *PCE* of 8.67%, with a short circuit current (J_{SC}) of 12.4 mA cm^{-2}, a V_{OC} of 1.16 V, and a fill factor (*FF*) of 60.1%. The device shows an external quantum efficiency (*EQE*) spectrum (Figure S6) above 60% from 390 to 620 nm. The integrated photocurrent from the *EQE* gives a J_{SC} of 12.1 mA cm^{-2}, which is in good agreement with the measured value from the *J-V* data. For the device annealed at 280°C, a *PCE* of 8.02% was obtained. Although the annealed-film device shows a higher J_{SC}, which is attributed to better carrier mobility and transport properties from the larger grain size (Senanayak et al., 2017), the loss of voltage leads to a slightly lower overall device performance. The V_{OC} of the 280°C film device is only 1.01 V, which is significantly lower than that of the room temperature device. We measured the photoluminescence (PL) spectra for the two films and found that the room temperature film shows a strong PL peak at 645 nm, and that the peaks shift to 655 nm (with a decrease in intensity) after being annealed to 280°C. This PL spectral shift could stem from an increase in defect state emission or development of charge transfer states and actually suggests that there is a lower defect density or a reduction in charge transfer states in the room temperature-processed film. The high V_{OC} of the room temperature device can be attributed to fewer defects (or possibly charge transfer states) and shunting pathways, which is confirmed by the stronger (and blueshifted) PL spectrum (Figure S7). It is also possible that the blueshift in the PL stems from very small grain size formation, which leads to a degree of quantum confinement and a potential increase in the bandgap (Figure S2B). In addition, the smooth film surface results in good contact between the perovskite film and the evaporated fullerene electron transfer layer, which also contributes to the improved V_{OC} over the annealed device. Figure 3C shows that the steady photocurrent and power output of room temperature device is 10.6 mA cm^{-2} and 8.30 mW cm^{-2} under a bias of 0.78 V, respectively. Moreover, the room temperature processed device only shows a small photocurrent hysteresis when measured under forward and reversed scan modes (Figure 3D).

Based on the room temperature processing technique, inorganic cesium lead halide perovskite device were prepared on flexible substrates (Figure 4A). An ITO/polyethylene terephthalate (PET) flexible substrate was used to replace the rigid ITO/glass substrate to prepare the flexible device. Figure 4B shows the *J-V* curve of the flexible cesium lead halide PSC. The flexible device shows a *PCE* of 6.50% under 1-sun illumination, with a J_{SC} of 12.0 mA cm^{-2}, a V_{OC} of 1.05 V, and an *FF* of 51.4%. The unencapsulated flexible device maintained an efficiency of 6.05% after 2 months storage in inert atmosphere, which is 93% of the original efficiency.

Bending tests were carried out to check the performance of flexible device after repeated bend cycles. After 100 bending cycles around a radius of 4.05 mm, the device only showed slight fluctuations in the efficiency (Figure 4C). However, the efficiency of the flexible device drops to ~80% after 200 bending circles,

largely due to drops in the *FF*, which likely stem from cracking of the ITO/PET flexible substrate. Although the performance of flexible inorganic PSC can still be improved, these first demonstrations are encouraging for the development of low-cost, flexible, and stable inorganic PSCs.

Conclusion

In this work, we demonstrate an approach to prepare inorganic lead perovskite films with a room temperature process. The room temperature film shows improved humidity stability over films prepared by high-temperature annealing treatment. Utilizing the room temperature approach, the inorganic lead PSCs are successfully prepared on rigid and flexible substrates. This work demonstrates the integration of inorganic halide perovskites into flexible solar cells and highlights the great potential of inorganic perovskite materials for a range of flexible optoelectronic devices.

METHODS

All methods can be found in the accompanying Transparent Methods supplemental file.

SUPPLEMENTAL INFORMATION

Supplemental Information includes Transparent Methods, seven figures, one table and can be found with this article online at https://doi.org/10.1016/j.isci.2018.08.005.

ACKNOWLEDGMENTS

The authors acknowledge financial support from the Michigan State University Strategic Partnership Grant (SPG) (D.L.) and from the U.S. Department of Energy (DOE) Office of Science, under Award # DE-SC0010472.

AUTHOR CONTRIBUTIONS

D.L. and R.R.L. conceived the project and designed the experiments. D.L. fabricated and tested the films and devices. C.Y. assisted with measuring the PL data. M. B. assisted with device measurements. All authors contributed to the discussion of the data. D.L. and R.R.L wrote the manuscript.

DECLARATION OF INTERESTS

D.L. and R.R.L. have filed a patent application based on the work in this manuscript. All other authors declare no competing financial interest.

Received: June 17, 2018
Revised: July 26, 2018
Accepted: August 7, 2018
Published: August 31, 2018

REFERENCES

Ahn, N., Son, D.-Y., Jang, I.-H., Kang, S.M., Choi, M., and Park, N.-G. (2015). Highly reproducible perovskite solar cells with average efficiency of 18.3% and best efficiency of 19.7% fabricated via Lewis base adduct of lead(II) iodide. J. Am. Chem. Soc. *137*, 8696–8699.

Akkerman, Q.A., Gandini, M., Di Stasio, F., Rastogi, P., Palazon, F., Bertoni, G., Ball, J.M., Prato, M., Petrozza, A., and Manna, L. (2016). Strongly emissive perovskite nanocrystal inks for high-voltage solar cells. Nat. Energy *2*, 16194.

Beal, R.E., Slotcavage, D.J., Leijtens, T., Bowring, A.R., Belisle, R.A., Nguyen, W.H., Burkhard, G.F., Hoke, E.T., and McGehee, M.D. (2016). Cesium lead halide perovskites with improved stability for tandem solar cells. J. Phys. Chem. Lett. *7*, 746–751.

Bi, C., Chen, B., Wei, H., DeLuca, S., and Huang, J. (2017). Efficient flexible solar cell based on composition-tailored hybrid perovskite. Adv. Mater. *29*, 1605900.

Burschka, J., Pellet, N., Moon, S.-J., Humphry-Baker, R., Gao, P., Nazeeruddin, M.K., and Gratzel, M. (2013). Sequential deposition as a route to high-performance perovskite-sensitized solar cells. Nature *499*, 316–319.

Chen, C.-Y., Lin, H.-Y., Chiang, K.-M., Tsai, W.-L., Huang, Y.-C., Tsao, C.-S., and Lin, H.-W. (2017). All-vacuum-deposited stoichiometrically balanced inorganic cesium lead halide perovskite solar cells with stabilized efficiency exceeding 11%. Adv. Mater. *29*, 1605290.

Chen, J., Xiong, Y., Rong, Y., Mei, A., Sheng, Y., Jiang, P., Hu, Y., Li, X., and Han, H. (2016). Solvent effect on the hole-conductor-free fully printable perovskite solar cells. Nano Energy *27*, 130–137.

Docampo, P., Ball, J.M., Darwich, M., Eperon, G.E., and Snaith, H.J. (2013). Efficient organometal trihalide perovskite planar-heterojunction solar cells on flexible polymer substrates. Nat. Commun. *4*, 2761.

Duan, J., Zhao, Y., He, B., and Tang, Q. (2018). High-purity inorganic perovskite films for solar cells with 9.72 % efficiency. Angew. Chem. Int. Ed. *130*, 3849–3853.

Eperon, G.E., Paterno, G.M., Sutton, R.J., Zampetti, A., Haghighirad, A.A., Cacialli, F., and Snaith, H.J. (2015). Inorganic cesium lead iodide perovskite solar cells. J. Mater. Chem. A *3*, 19688–19695.

Eperon, G.E., Stranks, S.D., Menelaou, C., Johnston, M.B., Herz, L.M., and Snaith, H.J. (2014). Formamidinium lead trihalide: a broadly tunable perovskite for efficient planar heterojunction solar cells. Energy Environ. Sci. *7*, 982–988.

Frolova, L.A., Anokhin, D.V., Piryazev, A.A., Luchkin, S.Y., Dremova, N.N., Stevenson, K.J., and Troshin, P.A. (2017). Highly efficient all-inorganic planar heterojunction perovskite solar cells produced by thermal coevaporation of CsI and PbI2. J. Phys. Chem. Lett. *8*, 67–72.

Gratzel, M. (2014). The light and shade of perovskite solar cells. Nat. Mater. *13*, 838–842.

Hao, F., Stoumpos, C.C., Guo, P., Zhou, N., Marks, T.J., Chang, R.P.H., and Kanatzidis, M.G. (2015). Solvent-mediated crystallization of CH3NH3SnI3 films for heterojunction depleted perovskite solar cells. J. Am. Chem. Soc. *137*, 11445–11452.

He, Q., Yao, K., Wang, X., Xia, X., Leng, S., and Li, F. (2017). Room-temperature and solution-processable Cu-doped nickel oxide nanoparticles for efficient hole-transport layers of flexible large-area perovskite solar cells. ACS Appl. Mater. Interfaces *9*, 41887–41897.

Hu, Y., Bai, F., Liu, X., Ji, Q., Miao, X., Qiu, T., and Zhang, S. (2017). Bismuth incorporation stabilized α-CsPbI3 for fully inorganic perovskite solar cells. ACS Energy Lett. *2*, 2219–2227.

Jeon, N.J., Noh, J.H., Kim, Y.C., Yang, W.S., Ryu, S., and Seok, S.I. (2014). Solvent engineering for high-performance inorganic–organic hybrid perovskite solar cells. Nat. Mater. *13*, 897.

Jo, Y., Oh, K.S., Kim, M., Kim, K.-H., Lee, H., Lee, C.-W., and Kim, D.S. (2016). High performance of planar perovskite solar cells produced from PbI2(DMSO) and PbI2(NMP) complexes by intramolecular exchange. Adv. Mater. Interfaces *3*, 1500768.

Kaltenbrunner, M., Adam, G., Głowacki, E.D., Drack, M., Schwödiauer, R., Leonat, L., Apaydin, D.H., Groiss, H., Scharber, M.C., White, M.S., et al. (2015). Flexible high power-per-weight perovskite solar cells with chromium oxide–metal contacts for improved stability in air. Nat. Mater. *14*, 1032.

Kojima, A., Teshima, K., Shirai, Y., and Miyasaka, T. (2009). Organometal halide perovskites as visible-light sensitizers for photovoltaic cells. J. Am. Chem. Soc. *131*, 6050–6051.

Lee, J., and Baik, S. (2018). Enhanced crystallinity of CH3NH3PbI3 by the pre-coordination of PbI2-DMSO powders for highly reproducible and efficient planar heterojunction perovskite solar cells. RSC Adv. *8*, 1005–1013.

Leijtens, T., Eperon, G.E., Noel, N.K., Habisreutinger, S.N., Petrozza, A., and Snaith, H.J. (2015). Stability of metal halide perovskite solar cells. Adv. Energy Mater. *5*, 1500963.

Li, K., Xiao, J., Yu, X., Li, T., Xiao, D., He, J., Zhou, P., Zhang, Y., Li, W., Ku, Z., et al. (2018). An efficient, flexible perovskite solar module exceeding 8% prepared with an ultrafast PbI2 deposition rate. Sci. Rep. *8*, 442.

Li, W., Rothmann, M.U., Liu, A., Wang, Z., Zhang, Y., Pascoe, A.R., Lu, J., Jiang, L., Chen, Y., Huang, F., et al. (2017). Phase segregation enhanced ion movement in efficient inorganic CsPbIBr2 solar cells. Adv. Energy Mater. *7*, 1700946.

Li, X., Bi, D., Yi, C., Décoppet, J.-D., Luo, J., Zakeeruddin, S.M., Hagfeldt, A., and Grätzel, M. (2016). A vacuum flash–assisted solution process for high-efficiency large-area perovskite solar cells. Science *353*, 58–62.

Liang, J., Wang, C., Wang, Y., Xu, Z., Lu, Z., Ma, Y., Zhu, H., Hu, Y., Xiao, C., Yi, X., et al. (2016). All-inorganic perovskite solar cells. J. Am. Chem. Soc. *138*, 15829–15832.

Ling, X., Yuan, J., Liu, D., Wang, Y., Zhang, Y., Chen, S., Wu, H., Jin, F., Wu, F., Shi, G., et al. (2017). Room-temperature processed Nb2O5 as the electron-transporting layer for efficient planar perovskite solar cells. ACS Appl. Mater. Interfaces *9*, 23181–23188.

Liu, D., Gangishetty, M.K., and Kelly, T.L. (2014). Effect of CH3NH3PbI3 thickness on device efficiency in planar heterojunction perovskite solar cells. J. Mater. Chem. A *2*, 19873–19881.

Liu, D., and Kelly, T.L. (2014). Perovskite solar cells with a planar heterojunction structure prepared using room-temperature solution processing techniques. Nat. Photon. *8*, 133–138.

Liu, D., Traverse, C.J., Chen, P., Elinski, M., Yang, C., Wang, L., Young, M., and Lunt, R.R. (2018a). Aqueous-containing precursor solutions for efficient perovskite solar cells. Adv. Sci. *5*, 1700484.

Liu, D., Wang, Q., Traverse, C.J., Yang, C., Young, M., Kuttipillai, P.S., Lunt, S.Y., Hamann, T.W., and Lunt, R.R. (2018b). Impact of ultrathin C60 on perovskite photovoltaic devices. ACS Nano *12*, 876–883.

Liu, M., Johnston, M.B., and Snaith, H.J. (2013). Efficient planar heterojunction perovskite solar cells by vapour deposition. Nature *501*, 395–398.

Luo, P., Xia, W., Zhou, S., Sun, L., Cheng, J., Xu, C., and Lu, Y. (2016). Solvent engineering for ambient-air-processed, phase-stable CsPbI3 in perovskite solar cells. J. Phys. Chem. Lett. *7*, 3603–3608.

Ma, Q., Huang, S., Chen, S., Zhang, M., Lau, C.F.J., Lockrey, M.N., Mulmudi, H.K., Shan, Y., Yao, J., Zheng, J., et al. (2017). The effect of stoichiometry on the stability of inorganic cesium lead mixed-halide perovskites solar cells. J. Phys. Chem. C *121*, 19642–19649.

Mei, A., Li, X., Liu, L., Ku, Z., Liu, T., Rong, Y., Xu, M., Hu, M., Chen, J., Yang, Y., et al. (2014). A hole-conductor–free, fully printable mesoscopic perovskite solar cell with high stability. Science *345*, 295.

Nam, J.K., Chai, S.U., Cha, W., Choi, Y.J., Kim, W., Jung, M.S., Kwon, J., Kim, D., and Park, J.H. (2017a). Potassium incorporation for enhanced performance and stability of fully inorganic cesium lead halide perovskite solar cells. Nano Lett. *17*, 2028–2033.

Nam, J.K., Jung, M.S., Chai, S.U., Choi, Y.J., Kim, D., and Park, J.H. (2017b). Unveiling the crystal formation of cesium lead mixed-halide perovskites for efficient and stable solar cells. J. Phys. Chem. Lett. *8*, 2936–2940.

Nie, W., Tsai, H., Asadpour, R., Blancon, J.-C., Neukirch, A.J., Gupta, G., Crochet, J.J., Chhowalla, M., Tretiak, S., Alam, M.A., et al. (2015). High-efficiency solution-processed perovskite solar cells with millimeter-scale grains. Science *347*, 522.

Niezgoda, J.S., Foley, B.J., Chen, A.Z., and Choi, J.J. (2017). Improved charge collection in highly efficient CsPbBrI2 solar cells with light-induced dealloying. ACS Energy Lett. *2*, 1043–1049.

Remeika, M., Ono, L.K., Maeda, M., Hu, Z., and Qi, Y. (2018). High-throughput surface preparation for flexible slot die coated perovskite solar cells. Org. Electron. *54*, 72–79.

Roldan-Carmona, C., Malinkiewicz, O., Soriano, A., Minguez Espallargas, G., Garcia, A., Reinecke, P., Kroyer, T., Dar, M.I., Nazeeruddin, M.K., and Bolink, H.J. (2014). Flexible high efficiency perovskite solar cells. Energy Environ. Sci. *7*, 994–997.

Senanayak, S.P., Yang, B., Thomas, T.H., Giesbrecht, N., Huang, W., Gann, E., Nair, B., Goedel, K., Guha, S., Moya, X., et al. (2017). Understanding charge transport in lead iodide perovskite thin-film field-effect transistors. Sci. Adv. *3*, e1601935.

Sharma, S., Weiden, N., and Weiss, A. (1992). Phase diagrams of quasibinary systems of the type: ABX3-A′BX3; ABX3-AB′X3, and ABX3-ABX′3; X = halogen. Z. Phys. Chem. *175*, 63–80.

Sutton, R.J., Eperon, G.E., Miranda, L., Parrott, E.S., Kamino, B.A., Patel, J.B., Hörantner, M.T., Johnston, M.B., Haghighirad, A.A., Moore, D.T., et al. (2016). Bandgap-tunable cesium lead halide perovskites with high thermal stability for efficient solar cells. Adv. Energy Mater. *6*, 1502458.

Swarnkar, A., Marshall, A.R., Sanehira, E.M., Chernomordik, B.D., Moore, D.T., Christians, J.A., Chakrabarti, T., and Luther, J.M. (2016). Quantum dot–induced phase stabilization of α-CsPbI3 perovskite for high-efficiency photovoltaics. Science *354*, 92.

Tsai, C.-M., Wu, G.-W., Narra, S., Chang, H.-M., Mohanta, N., Wu, H.-P., Wang, C.-L., and Diau, E.W.-G. (2017). Control of preferred orientation with slow crystallization for carbon-based mesoscopic perovskite solar cells attaining efficiency 15%. J. Mater. Chem. A *5*, 739–747.

Wang, C., Guan, L., Zhao, D., Yu, Y., Grice, C.R., Song, Z., Awni, R.A., Chen, J., Wang, J., Zhao, X., et al. (2017a). Water vapor treatment of low-temperature deposited SnO2 electron selective layers for efficient flexible perovskite solar cells. ACS Energy Lett. *2*, 2118–2124.

Wang, Q., Chen, B., Liu, Y., Deng, Y., Bai, Y., Dong, Q., and Huang, J. (2017b). Scaling behavior of moisture-induced grain degradation in polycrystalline hybrid perovskite thin films. Energy Environ. Sci. *10*, 516–522.

Wang, Q., Zheng, X., Deng, Y., Zhao, J., Chen, Z., and Huang, J. (2017c). Stabilizing the α-Phase of CsPbI3 perovskite by sulfobetaine zwitterions in one-step spin-coating films. Joule *1*, 371–382.

Wang, Y., Zhang, T., Xu, F., Li, Y., and Zhao, Y. (2017d). A facile low temperature fabrication of high performance CsPbI2Br all-inorganic perovskite solar cells. Solar RRL *2*, 1700180.

Wang, P., Zhang, X., Zhou, Y., Jiang, Q., Ye, Q., Chu, Z., Li, X., Yang, X., Yin, Z., and You, J. (2018). Solvent-controlled growth of inorganic perovskite films in dry environment for efficient and stable solar cells. Nat. Commun. *9*, 2225.

Wu, Y., Islam, A., Yang, X., Qin, C., Liu, J., Zhang, K., Peng, W., and Han, L. (2014). Retarding the crystallization of PbI2 for highly reproducible planar-structured perovskite solar cells via sequential deposition. Energy Environ. Sci. *7*, 2934–2938.

Yang, W.S., Park, B.-W., Jung, E.H., Jeon, N.J., Kim, Y.C., Lee, D.U., Shin, S.S., Seo, J., Kim, E.K., Noh, J.H., et al. (2017). Iodide management in formamidinium-lead-halide–based perovskite layers for efficient solar cells. Science *356*, 1376–1379.

Yin, W.-J., Yan, Y., and Wei, S.-H. (2014). Anomalous alloy properties in mixed halide perovskites. J. Phys. Chem. Lett. *5*, 3625–3631.

Yun, J.S., Kim, J., Young, T., Patterson, R.J., Kim, D., Seidel, J., Lim, S., Green, M.A., Huang, S., and Ho-Baillie, A. (2018). Humidity-induced degradation via grain boundaries of HC(NH2) 2PbI3 planar perovskite solar cells. Adv. Funct. Mater. *28*, 1705363.

Zeng, Q., Zhang, X., Feng, X., Lu, S., Chen, Z., Yong, X., Redfern, S.A.T., Wei, H., Wang, H., Shen, H., et al. (2018). Polymer-passivated inorganic cesium lead mixed-halide perovskites for stable and efficient solar cells with high open-circuit voltage over 1.3 V. Adv. Mater. *30*, 1705393.

Zhang, H., Cheng, J., Lin, F., He, H., Mao, J., Wong, K.S., Jen, A.K.Y., and Choy, W.C.H. (2016). Pinhole-free and surface-nanostructured NiOx film by room-temperature solution process for high-performance flexible perovskite solar cells with good stability and reproducibility. ACS Nano *10*, 1503–1511.

Zhang, J., Bai, D., Jin, Z., Bian, H., Wang, K., Sun, J., Wang, Q., and Liu, S. (2018a). 3D–2D–0D interface profiling for record efficiency all-inorganic CsPbBrI2 perovskite solar cells with superior stability. Adv. Energy Mater. *8*, 1703246.

Zhang, T., Dar, M.I., Li, G., Xu, F., Guo, N., Grätzel, M., and Zhao, Y. (2017). Bication lead iodide 2D perovskite component to stabilize inorganic α-CsPbI3 perovskite phase for high-efficiency solar cells. Sci. Adv. *3*, e1700841.

Zhang, Y., Wu, Z., Li, P., Ono Luis, K., Qi, Y., Zhou, J., Shen, H., Surya, C., and Zheng, Z. (2018b). Fully solution-processed TCO-free semitransparent perovskite solar cells for tandem and flexible applications. Adv. Energy Mater. *8*, 1701569.

Zhou, H., Chen, Q., Li, G., Luo, S., Song, T.-b., Duan, H.-S., Hong, Z., You, J., Liu, Y., and Yang, Y. (2014). Interface engineering of highly efficient perovskite solar cells. Science *345*, 542.

Zhou, Y., Yang, M., Wu, W., Vasiliev, A.L., Zhu, K., and Padture, N.P. (2015). Room-temperature crystallization of cybrid-perovskite thin films via solvent-solvent extraction for high-performance solar cells. J. Mater. Chem. A *3*, 8178–8184.

ISCI, Volume *6*

Supplemental Information

Room Temperature Processing of Inorganic Perovskite Films to Enable Flexible Solar Cells

Dianyi Liu, Chenchen Yang, Matthew Bates, and Richard R. Lunt

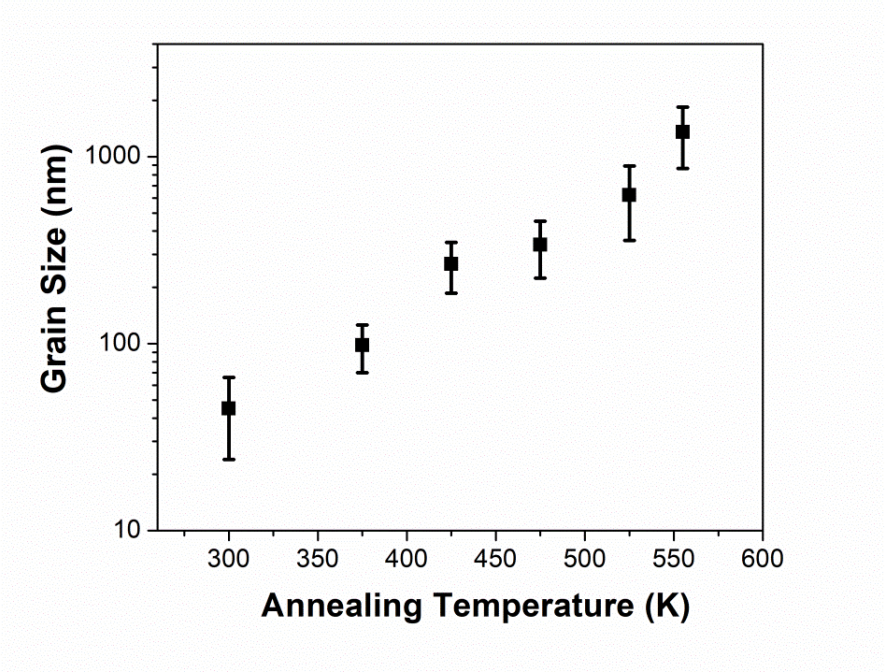

Figure S1. Grain size of $CsPbI_2Br$ film as a function of the annealing temperature, Related to Figure 1.

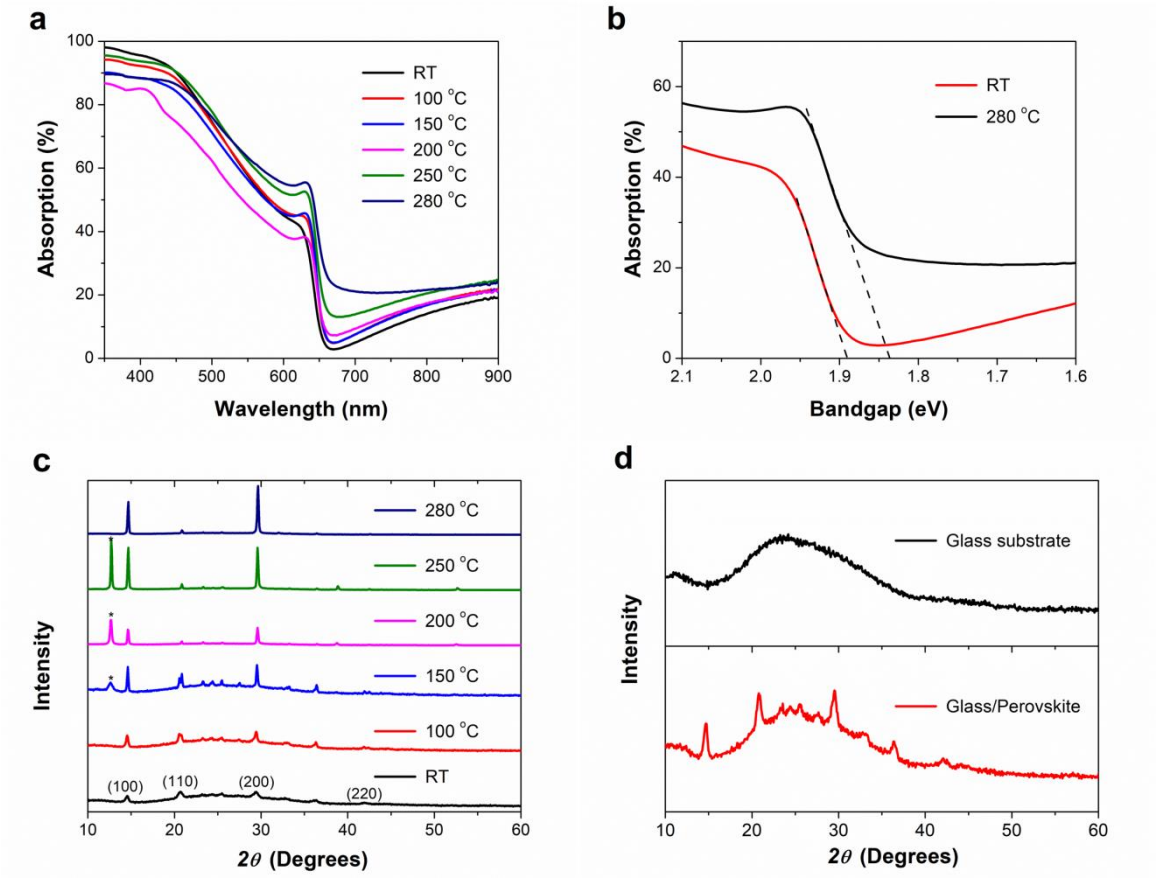

Figure S2. $CsPbI_2Br$ films characterization, Related to Figure 2. Absorption spectra (a) and XRD patterns (c) of $CsPbI_2Br$ films with various temperature treatments; (b) plot for $CsPbI_2Br$ bandgap measurement from optical absorption of room temperature and 280 °C films; (d) the comparison of XRD pattern of the glass substrate and perovskite film on glass substrate.

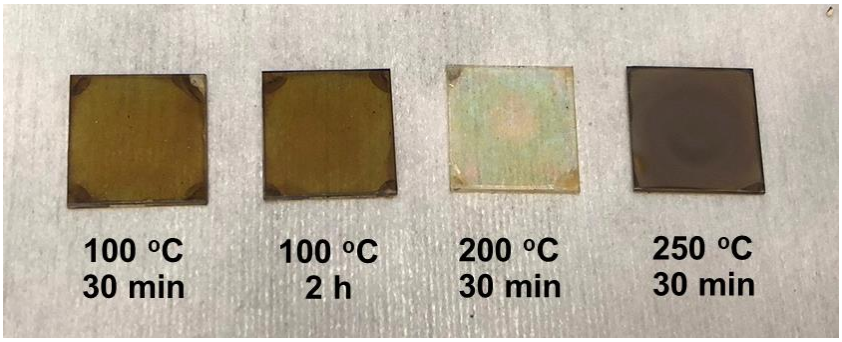

Figure S3. Photograph of $CsPbI_2Br$ films annealed with various temperatures and times, Related to Figure 2.

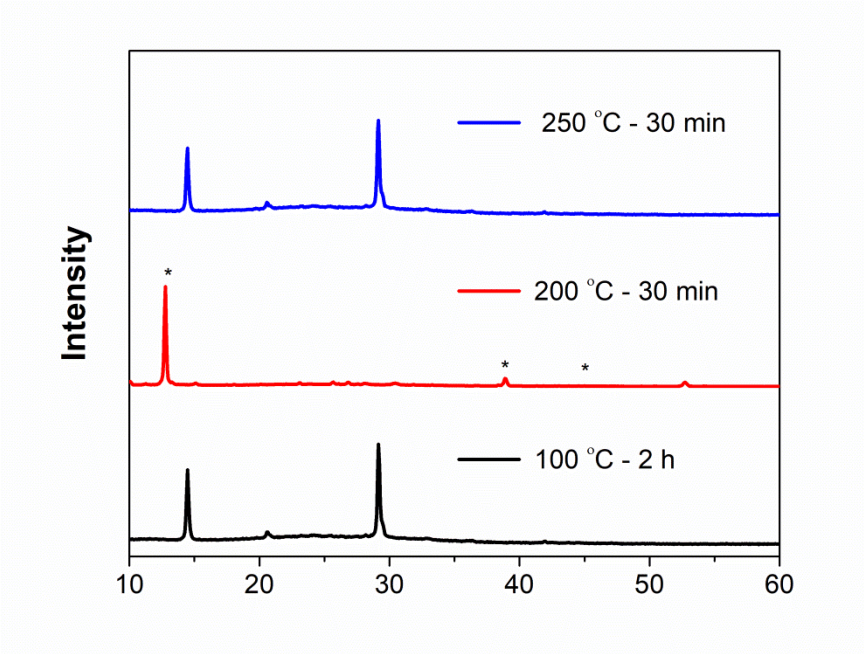

Figure S4. XRD pattern of $CsPbI_2Br$ films annealed with various temperatures and times, Related to Figure 2.

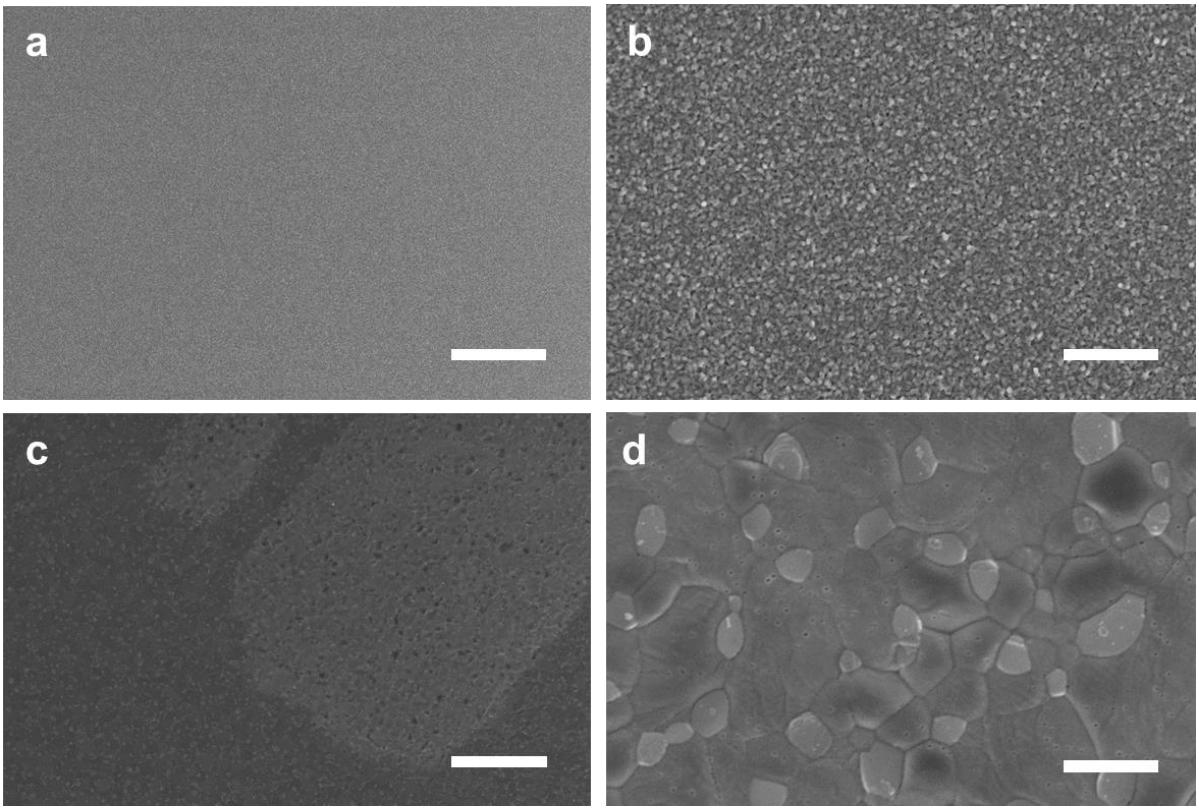

Figure S5. SEM images of $CsPbI_2Br$ film stored in ambient air (RH = 30 ± 4%) for 5 minutes, Related to Figure 2. (a) and (b) is the room temperature $CsPbI_2Br$ film; (c) and (d) is the 280 °C annealing treatment $CsPbI_2Br$ film. The scale bar is 10 μm for (a) and (c), 1 μm for (b) and (d), respectively.

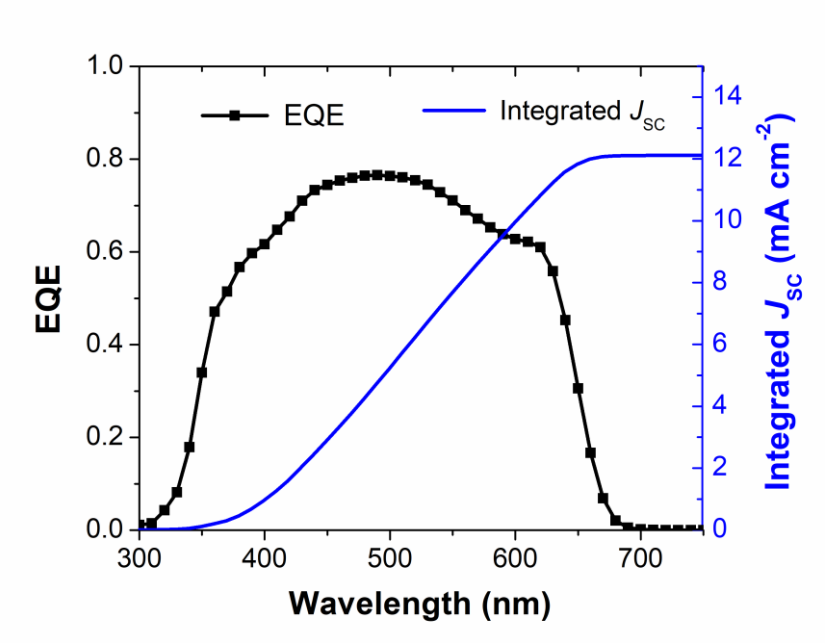

Figure S6. *EQE* spectrum of the room-temperature $CsPbI_2Br$ devices, Related to Figure 3. Left axis (black squares) is the measured *EQE* spectrum. Right axis (blue line) is the corresponding integrated *EQE* to give the cumulative short circuit photocurrent as a function of wavelength.

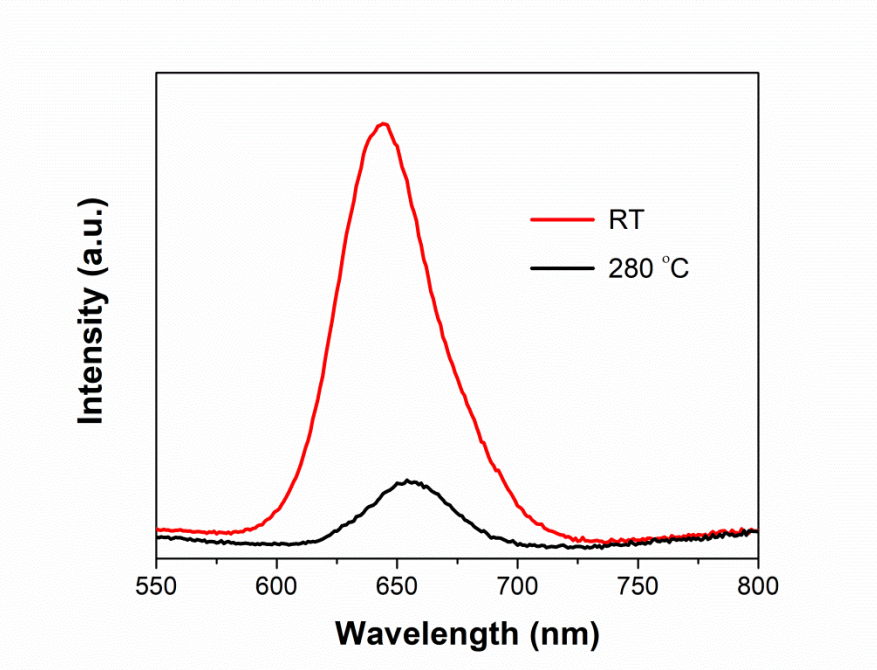

Figure S7. Photoluminescence spectra of $CsPbI_2Br$ films with various temperature treatments, Related to Figure 3.

Device	# of	J_{SC} [mA cm^{-2}]	V_{OC} [V]	*FF* (%)	*PCE* [%]
Room Temperature	37	12.0 ± 0.7	1.12 ± 0.03	52.0 ± 7.9	7.00 ± 1.1
280 °C Annealed	32	13.1 ± 1.3	0.906 ± 0.07	52.4 ± 5.8	6.14 ± 0.7

Table S1. Average device parameters for the $CsPbI_2Br$ devices from room temperature film and anneal film, Related to Figure 3.

Transparent Methods

Materials and Precursor Preparation: 1-methyl-2-pyrrolidone (NMP, anhydrous, 99.5%, Aldrich.), dimethylformamide (DMF, anhydrous, 99.8%, Sigma Aldrich), dimethyl sulfoxide (DMSO, anhydrous, 99.9%, Sigma Aldrich), PEDOT:PSS (Clevios PVP AI 4083, Heraeus, diluted to 5% with water), PbI_2 (99%, Sigma Aldrich), CsBr (99.999%, Sigma Aldrich.), C_{60} (99.9%, MER Corporation.) and 2,9-dimethyl-4,7-diphenyl-1,10-phenanthroline (BCP, Lumtech) were used as received.

To prepare the perovskite precursor solution, PbI_2: CsBr (461 mg and 213 mg, respectively) were added in NMP (1.2 ml). The solutions were stirred for 1 hour and filtered with 0.45 μm PTFE filters before use.

Device Fabrication: The PEDOT layer and inorganic perovskite layer were prepared under open air conditions (with a measured relative humidity ≤ 36 ± 4%). The PEDOT solution was spin-coated onto pre-cleaned ITO substrates at 6000 rpm for 20 s. The perovskite precursor was spin-coated on top of the PEDOT film at 6000 rpm for 12 s, and then moved the substrate into a homemade vacuum chamber, evacuated to ~ 10 mtorr, and left in the chamber for 3 min. The samples were then transferred into glovebox. For high-temperature films, the substrates were annealed to 260-280 °C for 1 min. The substrates were then moved into the evaporation chamber for deposition of C_{60} (20 nm) and BCP (7.5 nm). Finally, an 80 nm thick silver layer was deposited by thermal evaporation at a base pressure of 3×10^{-6} Torr through a shadow mask with a final measured device area of 4.85 mm^2.

Measurement and Characterization: The current density–voltage characteristics (*J–V* curves) were obtained using a Keithley 2420 sourcemeter under AM1.5 G solar simulation (xenon arc lamp with the spectral-mismatch factor of 0.980.) where the light intensity was measured using a NREL-calibrated Si reference cell with KG5 filter. For devices with annealing treatment, the devices were encapsulated in epoxy in glovebox before being tested due to their sensitivity to air. The room temperature films and devices, include the flexible devices, were generally tested under ambient air condition (the RH ≤ 36 ± 4%) without any protection or encapsulation. Devices were scanned at a rate of 50 mV s^{-1}. The *EQE* measurements were performed using a QTH lamp with a monochromator, chopper, lock-in amplifier, and calibrated Si detector to measure the intensity. XRD data was measured using CuKα (0.154 nm) emission with a Bruker D2 phaser. The *UV-vis* and XRD were measured on un-encapsulated samples with glass substrates in ambient air (the relative humidity ≤ 22 ± 4%). A field-emission scanning electron microscopy (Carl Zeiss Auriga Dual Column FIB SEM) was used to acquire SEM images.